JOURNAL OF MATERIALS SCIENCE 31 (1996) 4087–4092

Anisotropy of crystallite growth during sintering of SnO_2 xerogels

G. E. S. BRITO, S. H. PULCINELLI, C. V. SANTILLI
Instituto de Química, UNESP, P.O. Box 355, Araraquara, SP, 14800-900, Brazil

The crytallite and pore-size evolution during isothermal sintering ($400 \leqslant T \leqslant 700\,^{\circ}C$) of SnO_2 xerogels was studied by X-ray line broadening and nitrogen adsorption–desorption isotherms. The experimental results show a strong anisotropy of crystallite growth between [1 1 0] and [1 0 1] directions. The preferential growth at [1 0 1] is followed by an increase in the mean pore size, reduction of the specific surface area and invariance of total pore volume. This behaviour is typical of grain coalescence sintering. The kinetic analysis of experimental results suggests that the crystallite coalescence at [1 0 1] is governed by lattice diffusion. The strong anisotropy of the growth causes pore-size distribution broadening, hindering the macroscopic shrinkage of the compact during sintering.

1. Introduction

Some unique properties of SnO_2 make this material useful for many potential applications such as static-charge elimination coatings, passivation layers of electronic components, transparent electrodes, gas sensors and ultrafiltration membranes [1–4]. Because of this wide range of applications sol–gel pathways to prepare SnO_2-based materials have received some attention in recent years [5, 6]. Less attention has been paid to understand the main structural transformations involved during the sintering of SnO_2 xerogels.

There is now ample evidence that, during the sintering of non-crystalline solids prepared by the sol–gel method, at least four mechanisms contribute to shrinkage leading to the total densification of the xerogel at low temperatures [7]. On the contrary, for the specific case of microcrystalline xerogels of SnO_2, pore and particle growth is the main phenomenon observed during sintering [8]. Recently, we showed by *in situ* small-angle X-ray scattering (SAXS) measurements that the SnO_2 xerogels exhibit a dynamical scaling growth governed by a diffusional process of pore coagulation [9]. Meanwhile, the mechanism of transport of material which governs this process has not yet been established.

Several mechanisms have been proposed to explain the observed pore and grain growth in SnO_2 ceramics prepared by classical routes. Some authors have attributed this phenomenon to processes controlled by diffusion, whereas others affirm it is due to non-diffusional ones. Quadir and Readey [10] have proposed that the Ostwald ripening process for particles growth, which is controlled by diffusion in the liquid phase, is responsible for the anisotropic grain growth during SnO_2 sintering under a hydrogen atmosphere. Goodman and Gregg [11] suggested that grain coalescence results from viscous flow at the grain boundaries owing to the movement of dislocations. Joss [12] and Varela *et al.* [13] proposed that this phenomenon is controlled by evaporation–condensation due to the reduction of SnO_2 into SnO(g). Nevertheless, thermodynamical calculations performed by Dolet [14] showed that at 1100 °C the partial pressure of SnO(g) in equilibrium with SnO_2 is smaller than 9×10^{-9} atm. This extremely small value makes the effective participation of SnO(g) questionable during the grain-growth process. Sharigin *et al.* [15] proposed that the enlargement of the primary crystalline particles is due to a mechanism of crystallization–aggregation, which involves a non-diffusional process of aggregation of particles of adjacent crystallographic planes caused by a complex stress state.

Although the proposed mechanisms are distinct from each other, all the authors mentioned above take account of the high anisotropy peculiar to the tetragonal structure of rutile-type to justify the phenomenon of grain growth during the sintering of SnO_2. Meanwhile, the literature does not reveal a kinetic study of the grain growth at the distinct crystallographic directions for SnO_2. The aim of the present work was to analyse the kinetics of the anisotropic grain growth between directions [1 1 0] and [1 0 1]. Information about the transport mechanism which governs the growth process has been obtained by using the classical relationship proposed by Lifshitz and Slyozov [16].

$$G^n - G_0^n = k \cdot t \qquad (1)$$

where G_0 is the initial average particle radius, G is the average radius at time t of treatment, and k is the rate constant which is proportional to the diffusivity

0022–2461

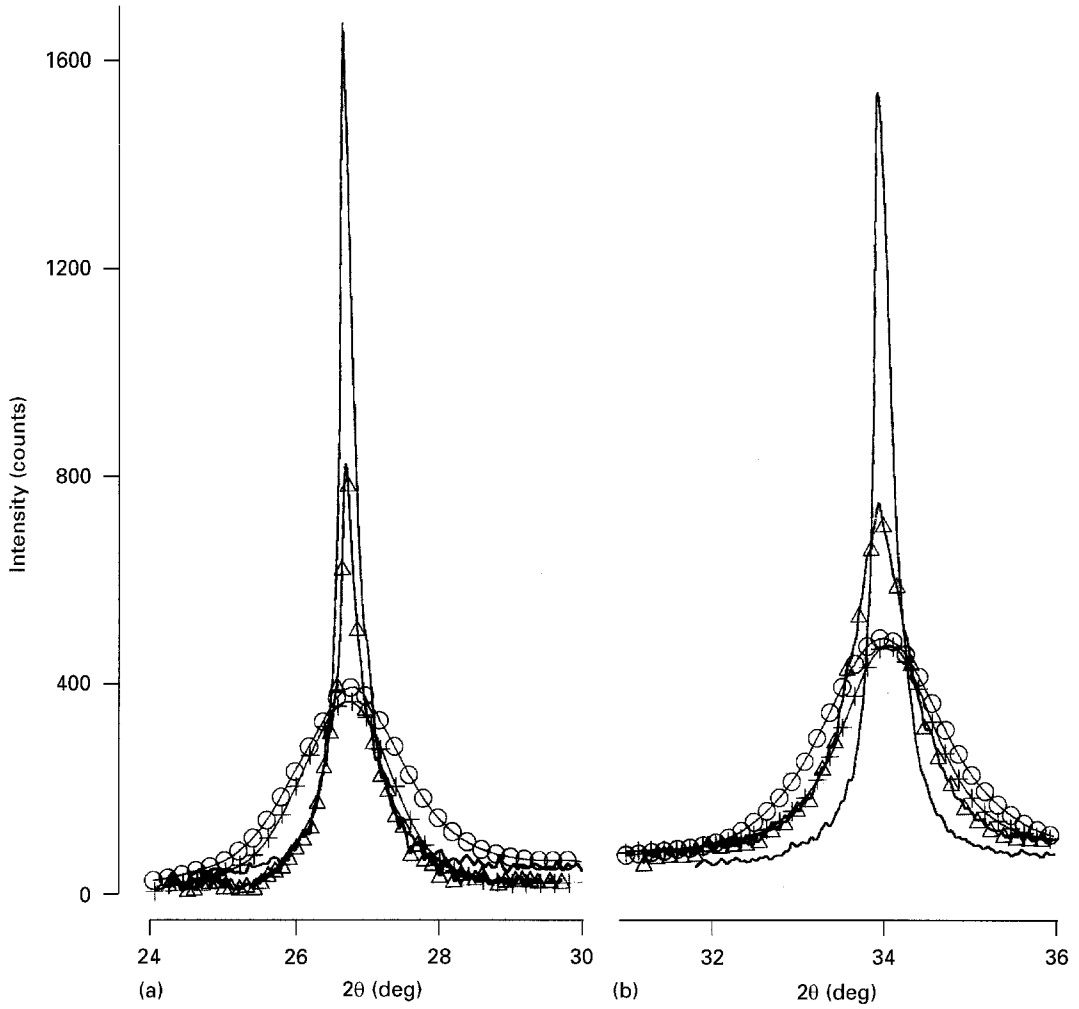

Figure 1 Evolution of X-ray diffraction profiles on (a) [1 1 0] and (b) [1 0 1] with sintering temperature during 180 min: (○) 400 °C, (+) 500 °C, (△) 600 °C, (——) 700 °C.

and to the activation energy of the transport process. The value of the exponent n is characteristic of the mechanism responsible for growth. In addition, assuming that grain growth in crystals is controlled by pore migration, Nichols [17] has showed that n is equal to 4 for growth governed by volume diffusion or vapour transport, increasing to 5 when diffusion along the surface or grain boundary is controlling.

2. Experimental procedure

2.1. Preparation of samples

A very fine SnO_2 powder (surface area = 162 $m^2 g^{-1}$), prepared by the sol–gel process [5], was used in this investigation. The powdered xerogel was isostatically pressed at 210 MPa to obtain pellets of 13 mm diameter and 3 mm thick. Isothermal sintering of these pellets was carried out at 400, 500, 600 and 700 °C in a furnace with an alumina tube chamber. The samples put inside an alumina boat were preheated at 300 °C for 15 min; then the boat was pushed into the hot zone of the furnace using an alumina rod. The zero time of sintering was defined when the furnace had reached the thermal equilibrium after the introduction of the boat into the hot zone; thermal equilibrium took about 3 min.

2.2. Crystallite size measurements

The mean crystallite size, G, was determined by using the Fourier real coefficients, A, calculated from the true X-ray diffraction line profiles obtained after background, Lorentz and polarization corrections [18]. The mean crystallite size is given by the initial slope of the $A(L)$ versus L curve [19]

$$\frac{1}{G_{hkl}} = \frac{dA(L)}{dL} \quad (2)$$

where L is the distance normal to the reflecting planes $(h\,k\,l)$. The Fourier coefficients were calculated by using the Stokes method and the k_{α_2} contribution to each peak eliminated by the Rachinger's correction. The X-ray diffraction patterns were recorded by using a HZG-4C, Carl–Zeiss equipment, nickel-filtered CuK_α radiation (λ = 0.15418 nm), and the diffraction peaks [1 1 0] and [1 0 1] were collected by step scanning mode (step = 0.05° and time = 50 s).

2.3. Specific area and porosity measurements

The specific surface area and porosity were determined by the analysis of the nitrogen adsorption–desorption isotherms, measured at 77 K in an

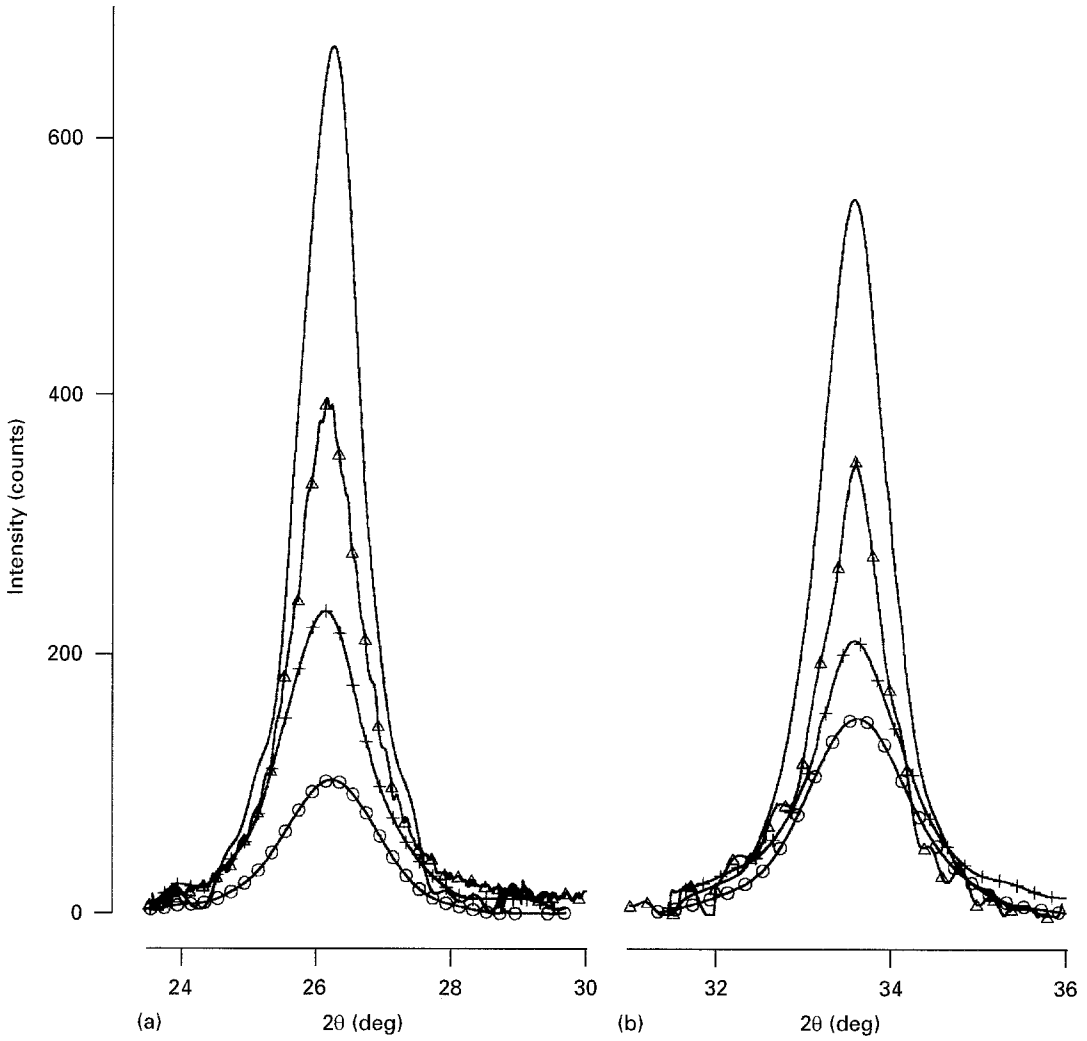

Figure 2 Evolution of the X-ray diffraction profiles on (a) [1 1 0] and (b) [1 0 1] with sintering time at 500 °C: (○) 10 min, (+) 30 min, (△) 90 min, (——) 360 min.

ASAP2000, Micrometers equipment. The measurements were accomplished after degas pre-treatment of the samples, carried out at 100 °C under 10^{-3} mm Hg vacuum for approximately 15 h. The specific area, S, and pore-size distribution were determined by BET and BJH methods [20], respectively.

3. Results

Figs 1 and 2 present the evolution of the X-ray diffraction profiles at [1 1 0] and [1 0 1] with the temperature of sintering, T_s, for the samples treated for 180 min and with the time of sintering, t_s, at 500 °C, respectively. The peak width decreases as T_s increases, indicating crystallite growth; this phenomenon is more intense at [1 0 1].

The analysis of the Fourier coefficients allowed calculation of the contributions of crystallite growth and microstrains into the peak profile broadening. All the samples show a microstrain rate smaller than 10^{-6}. So, the mean crystallite size, G, was determined directly from the Fourier coefficients curves $A(L)$ versus L, shown in Fig. 3. The initial slope of the curves remains essentially constant, for [1 1 0] reflections and decreases as t_s increases for [1 0 1] indicating preferential growth of crystallite size in this direction. Similar behaviour was observed for the samples treated at 600 and 700 °C. In addition, the hook effect was not present at small L values, showing the background and other instrumental effects were adequately corrected and allowing good accuracy in G values.

The log–log plot of mean crystallite size calculated for the [1 1 0] and [1 0 1] directions as a function of time for samples sintered at several temperatures, is presented in Fig. 4. For [1 1 0], the crystallite size is almost time-independent during sintering and the slope of the curves is 0.04. On the other hand, on [1 0 1] a considerable crystallite size growth is observed. The least square fitting of the experimental values by straight lines, makes it apparent that the slopes (0.25) are almost constant for all sintering temperatures. This suggests that the process limiting crystallite growth is the same for all the temperatures considered. It allows determination, for each temperature, of the values of the constant rate, k, of crystallite growth from the slope of the plot $G^{-0.25}$ versus sintering time.

Fig. 5 presents the Arrhenius plot of the rate constant of crystallite growth on [1 0 1] as a function of reciprocal temperature. The activation energy calculated from the slope of the straight line is 150 kJ mol^{-1}.

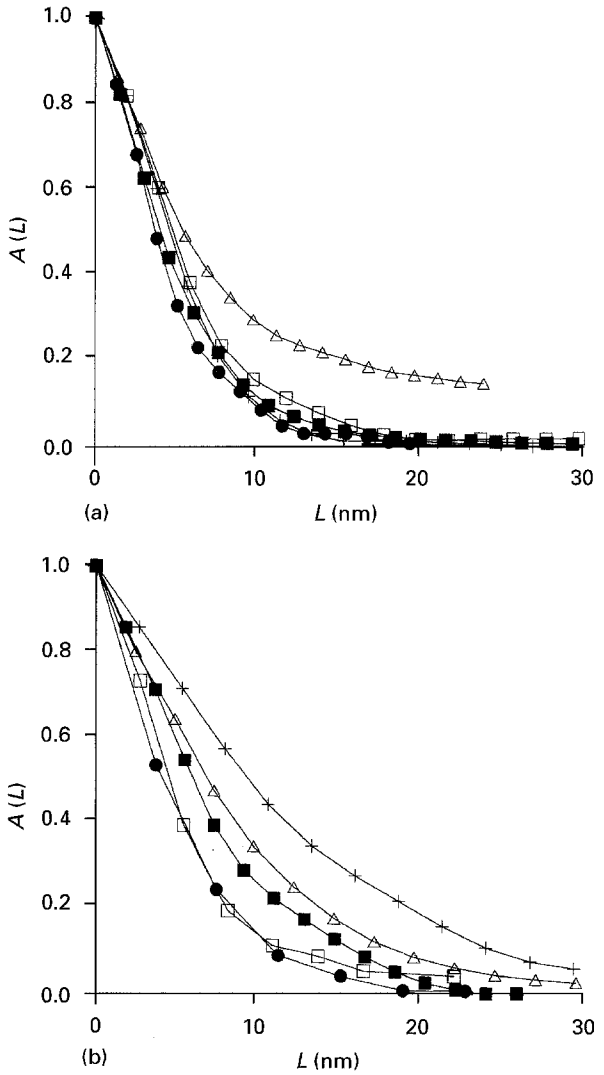

Figure 3 Fourier coefficient curves for (a) [1 1 0] and (b) [1 0 1] line profiles for samples sintered at 500 °C during: (●) 10 min, (□) 30 min, (■) 90 min, (△) 180 min, (+) 360 min.

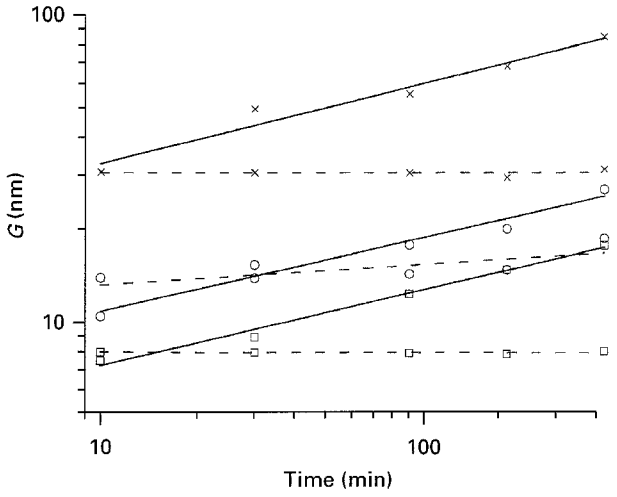

Figure 4 Log–log plot of the mean crystallite size on (----) [1 1 0] and (——) [1 0 1] as a function of time for samples sintered at (□) 500 °C, (○) 600 °C, (×) 700 °C.

The evolution of the pore-size distribution with sintering temperature is presented in Fig. 6a, for samples treated for 180 min and, with sintering time at 500 °C, in Fig. 6b. It can be observed that the mean

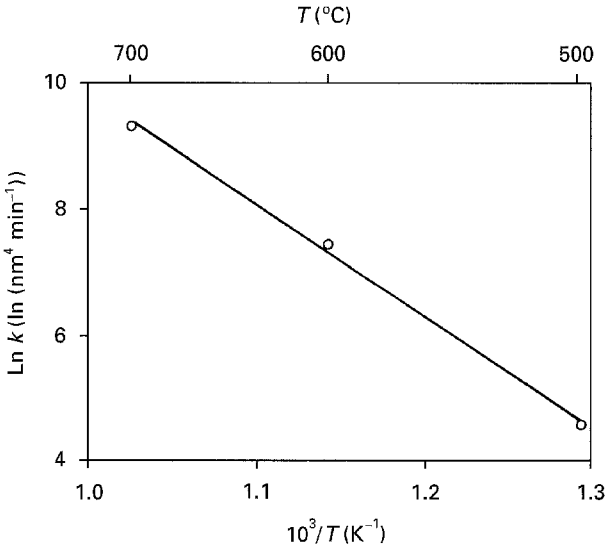

Figure 5 Arrhenius plot of the rate constant of crystallite growth on [1 0 1] as a function of the reciprocal temperature.

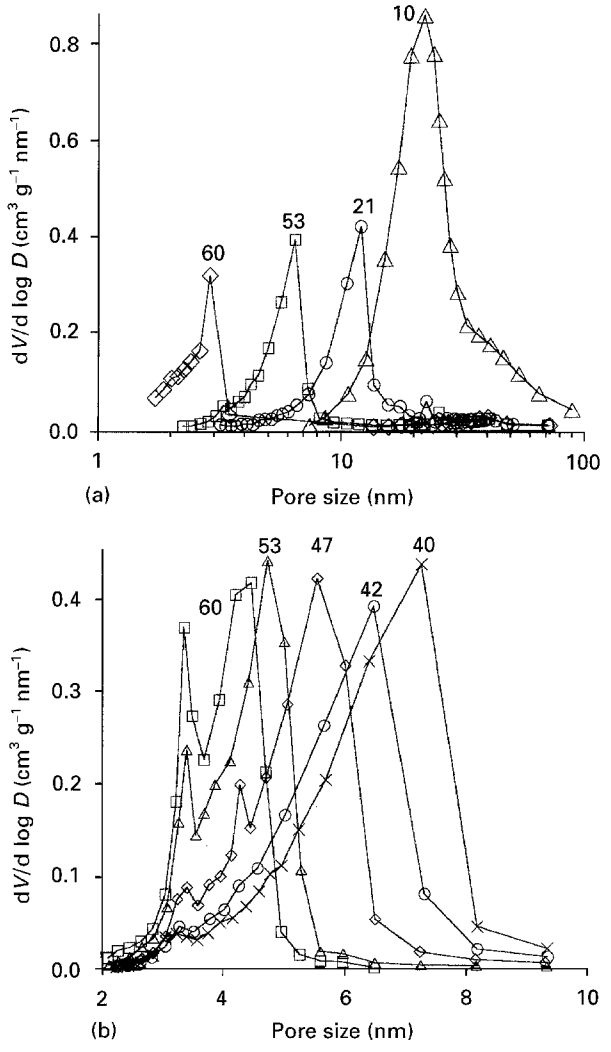

Figure 6 Evolution of the pore-size distribution (a) with sintering temperature during 180 min, and (b) with sintering time at 500 °C. The values of the specific surface area ($m^2 g^{-1}$) are given near the pore-size distribution. (a) (◇) 400 °C, (□) 500 °C, (○) 600 °C, (△) 700 °C, (b) (□) 10 min, (△) 30 min, (◇) 90 min, (○) 180 min, (×) 360 min.

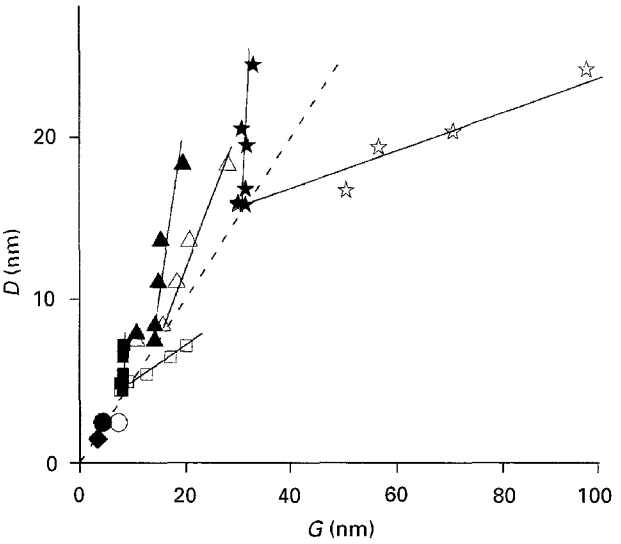

Figure 7 Evolution of the mean pore size, D, with the mean crystallite size, G, on the (◆, ●, ■, ▲, ★) [1 1 0], and (○, □, △, ☆) [1 0 1] directions. (- - - -) The linear dependence between D and G previewed for isotropic coalescence. (◆) 300 °C, (●, ○) 400 °C, (■, □) 500 °C, (▲, △) 600 °C, (★, ☆) 700 °C.

pore size and the distribution width increase as T_s and t_s increase. Moreover, the analysis of the adsorption isotherm reveals that the total pore volume of the compact (0.08 $cm^3 g^{-1}$) is practically constant during sintering, whereas the specific surface area (values given in Fig. 6) decreases as T_s and t_s increase.

Fig. 7 shows the evolution of the mean pore size, D, with the crystallite size in [1 1 0], and [1 0 1] directions. The least square fitting of the experimental values obtained for the samples sintered for 10 min, in which the anisotropy of size between these two directions is not pronounced, is also shown by the dashed line. This linear dependence, $D \propto G$, indicates that particle packing exhibits no significant alteration during the first instants of sintering.

4. Discussion

The analysis of the kinetics of crystallite growth in the [1 0 1] direction (Fig. 4) reveals that the exponent of Equation 1 assumes the value 4, which is characteristic of a growth mechanism governed by evaporation–condensation or by lattice diffusion. The predominance of the first mechanism depends on the equilibrium conditions established between SnO_2(s) and the eventual gas species SnO(g) and O_2. Thermodynamical calculation performed by Dolet [14], by considering a planar surface of evaporation and $p_{O_2} = 0.21$ atm, shows that for temperatures up to 700 °C, the equilibrium partial pressure of SnO(g) is smaller than 10^{-16} atm. Meanwhile, the small crystallite size of the SnO_2 samples prepared for this work could produce an increase in the vapour pressure. So, by using the Kelvin equation and considering spherical surfaces of 4 nm, which is equivalent to the observed crystallite size after 10 min sintering at 400 °C, we have estimated that $p_{SnO(g)}$ is almost 200 times

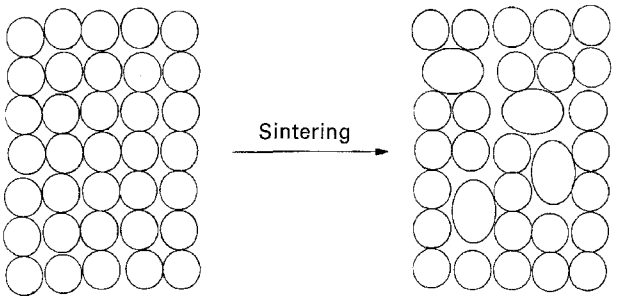

Figure 8 Change in local particle packing due to sintering (schematic proposition).

higher than the values obtained for a planar surface. Nevertheless, the values of $p_{SnO(g)}$ remain extremely small, hindering the attribution of the crystallite growth to the mechanism of evaporation–condensation.

On the other hand, there appears to be no published information on the diffusion coefficients in SnO_2, hindering a direct correlation between the activation energy for crystallite growth and a specific mechanism of transport. Meanwhile, it has been qualitatively demonstrated that the rutile-type structure of SnO_2 favours a preferential diffusion of interstitial cations and of oxygen vacancies along the c-axis [21]. In TiO_2, for example [21], the activation energy associated with diffusion of defects parallel to the c-direction is of the order of 80–100 kJ mol^{-1}. This small value is qualitatively comparable to the activation energy of 150 kJ mol^{-1} observed for the preferential crystallite growth on [1 0 1] for SnO_2 (Fig. 5).

This set of results allows the proposition that the diffusion of defects by the lattice is the mechanism which governs the crystallite growth observed between 500 and 700 °C. In general, this transport mechanism causes a reduction in the total pore volume and shrinkage of the compact, which is not observed for SnO_2. Otherwise, if, in some preferential direction, some particle pairs could sinter at a much greater rate than average, the approximation between the centre of adjacent particles does not result in macroscopic shrinkage. As shown in Fig. 8, this behaviour leads to a change in local particle packing and an increase in the size of neighbouring pores. Consequently, the pore-size distribution broadens (Fig. 6) and the particle size/pore size ratio varies, causing deviation from the linear behaviour of $D \propto G$ previewed (Fig. 7) for the isotropic grain coalescence.

It should be emphasized that, phenomenologically, the above proposition is analogous to the model termed fast-pairs, proposed by Sipe [22] to explain the pore growth observed during the initial stages of sintering of α-Fe_2O_3. He was able to prove the existence of fast sintering pairs from diffusion coefficients measurements, which revealed changes of a factor of 10^3 between different particle pairs. Meanwhile, the reasons involved in this behaviour are not stated. In this way, the results obtained for the crystallite growth of SnO_2 allowed this phenomenon to be attributed to the strong diffusion anisotropy, contributing to the

elucidation of the mechanism of particle coalescence proposed by Sipe.

5. Conclusion

The phenomenon of grain and pore coalescence during the sintering of SnO_2 xerogels results from the preferential crystallite growth in the [1 0 1] direction. For sintering temperatures between 500 and 700 °C, the crystallite growth is governed by lattice diffusion. The strong anisotropy of growth causes a broadening of the pore-size distribution, hindering shrinkage of the compact.

Acknowledgements

This work was supported by FAPESP and CNPq, Brazil.

References

1. W. A. BADWAY, *J. Electroanal. Chem.* **281** (1990) 85.
2. C. GEOFFROY, G. CAMPET, F. MENIL, J. PORTIER, J. SALARDENNE and G. COUTURIER, *Active Passive Elec. Comp.* **14** (1991) 111.
3. Z. M. JARZEBSKI and J. P. MARTON, *J. Electrochem. Soc. Rev. News* **123** (1976) 1990.
4. G. E. S. BRITO, S. H. PULCINELLI and C. V. SANTILLI, *J. Sol-Gel. Sci. Technol.* **2** (1994) 575.
5. R. S. HIRATSUKA, S. H. PULCINELLI and C. V. SANTILLI, *J. Non-Cryst. Solids* **121** (1990) 76.
6. R. T. PRESECATAN, S. H. PULCINELLI and C. V. SANTILLI, *ibid.* **147/148** (1992) 340.
7. J. BRINKER, G. W. SHERRER and E. P. ROTH, *J. Non-Cryst. Solids* **72** (1985) 345.
8. G. E. S. BRITO, S. H. PULCINELLI, C. V. SANTILLI and N. BARELLI, *J. Mater. Sci.* **12** (1993) 992.
9. A. CRAIEVICH, C. V. SANTILLI and S. H. PULCINELLI, *Nucl. Instrum. Meth. Phys. Res. B*, **97** (1995) 78.
10. T. QUADIR and D. W. READEY, in "Sintering and Heterogeneous Catalysis", edited by G. C. Kuezynski (Plenum Press, New York, 1984) p. 159.
11. J. F. GOODMAN and S. J. GREGG, *J. Chem. Soc.* **82** (1960) 1162.
12. H. D. JOSS, Master Thesis, University of Washington (1975).
13. J. A. VARELA, O. J. WHITTEMORE and M. J. BALL, in "Sintering 85", edited by G. C. Kuezynski, D. P. Uskokovic, H. Palmour and M. M. Ristic (Plenum Press, New York, 1987) p. 259.
14. N. DOLET, These de l'Université de Bordeaux I, no. 742 (1992).
15. L. M. SHARYGIN, V. F. GONCHAR and V. I. BORYBIN, *Izv. Akad. Nauk. SSSR Neorg. Mater.* **17** (1981) 1804.
16. I. M. LIFSCHITZ and V. V. SLYOZOV, *J. Phys. Chem. Solids* **19** (1961) 35.
17. F. A. NICHOLS, *J. Appl. Phys.* **37** (1966) 4599.
18. H. P. KLUG and L. E. ALEXANDER, "X-ray Diffraction Procedures for Polycrystalline and Amorphous Materials" (Wiley, New York, 1974).
19. P. H. DUVIGNEAUD and R. DERIE, *J. Solid State Chem.* **34** (1980) 323.
20. S. J. GREGG and K. S. W. SING, "Adsorption Surface Area and Porosity" (Academic Press, London, 1982).
21. P. KOFSTAD, "Nonstoichiometry, Diffusion and Electrical Conductivity in Binary Metal Oxides" (Wiley, New York, 1982) reprinted edition.
22. J. J. SIPE, PhD thesis, University of Washington (1971).

Received 22 December 1994
and accepted 13 February 1996